Multiphysics Modeling and Optimization of a Compact Actuation System

Florent Robert, Mohamed Bensetti, Filipe Vinci dos Santos, Laurent Dufour, Philippe Dessante

Multiphysics modeling and optimization of a compact actuation system

Florent Robert, *Member, IEEE*, Mohamed Bensetti, Filipe Vinci dos Santos, Laurent Dufour and Philippe Dessante

***Abstract*— This paper describes a methodology for the optimization of complex actuation systems, using analog simulations and an evolutionary algorithm. Our proposal consists on the development of an automated design framework that helps the designer to quickly complete a pre-sizing step while ensuring that multi-domain requirements are met within short development times typical of automotive industry. Multiphysics constraints can be handled, allowing the sizing of a complete automotive mechatronic system. The effectiveness of the methodology is demonstrated in the case of an exhaust gas recirculation (EGR) valve. Electrical, mechanical, thermal and magnetic requirements are met while a minimal volume is reached.**

***Index Terms*— Automotive, Electrical Drive, Optimization, Multiphysics, Smart actuator, System.**

I. Introduction

CAR manufacturer are expected to design cleaner and more efficient vehicles than in the past. International standards, such as EURO6 [1], impose tougher pollutant emission limits. Consumers are looking for greater comfort and fuel efficiency. To meet these challenges, cars have become increasingly complex platforms integrating many subsystems. These subsystems must satisfy the required purposes, coexist with all others and to be optimally designed. Compact actuators are one of such a subsystem that is widely used in automotive applications. The design of these actuators entails the concurrent development of the electromechanical assembly (actuator), power electronics converter, EMC (Electro Magnetic Compatibility) filter and loop control algorithm. This is a challenging task, for each of these is typically handled in separated modeling domains.

The literature abounds with examples where optimization algorithms are used for the design of elementary functional subsystems. In [2], authors succeeded in sizing a DC machine dedicated to an automotive application. Furthermore, in [3], a power converter is defined using an optimization algorithm, taking into account the EMC constraints. These studies report some interesting results and they outline a global approach which can be adopted by engineers in their daily tasks. In both cases, the analytical approach allows a relatively fast simulation run. This feature is all the most important in the sizing of a global system, where many parameters and interactions must be considered. However, the sizing of the machine and the converter are rarely considered simultaneously in the same approach.

Nevertheless, optimization of a multiphysics system by simulation remains difficult and expensive, since each simulation run takes significant computing time, and an optimization process relies on a huge number of runs. The computing time needed by an optimization algorithm for sizing of complex multiphysics system is generally regarded as prohibitive for industry adoption. Considering the current time to market expectations in the automotive industry, a designer should be able to pre-size the system in less than one week. Using optimization algorithms, a shorter development time is to be hoped, while achieving a greater accuracy due to the extent of the physical domains considered. Although the time spent to create and validate a model can appear to be a hindrance to the adoption of our automated approach, once the generic models are integrated into the multiphysics framework, any user can confidently pre-size similar parts.

In this paper, the authors show how an optimization process can be effectively applied to the sizing of a complete actuation system. This is a kind of multiphysics system because it must satisfy constraints and requirements across several physical domains. The effectiveness of the methodology is demonstrated in the case of an exhaust gas recirculation (EGR) valve.

In the following section, the EGR valve function and structure are described, the hypothesis used in our modeling are discussed and several physical models are introduced. In the third section, the optimization algorithm is applied in order to minimize the volume of the system under thermal and performances constraints, simultaneously taking into account EMC requirements. Lastly, the optimization results are discussed.

Manuscript received December 14, 2016; revised March 07, 2017 and March 28, 2017; accepted April 9, 2017.

F. Robert and L. Dufour are with the Research Department, EFi Automotive, Miribel, 01708 France (e-mail: florent.robert@efiautomotive.com; laurent.dufour@efiautomotive.com).

M. Bensetti and Ph. Dessante are with the Group of electrical engineering of Paris (GeePs), Gif-sur-Yvette, 91192 France (e-mail: philippe.dessante@centralesupelec.fr; mohamed.bensetti@centralesupelec.fr).

F. Vinci dos Santos is with the Chair on Advanced Analog Systems at CentraleSupélec, Gif-sur-Yvette, 91192 France (e-mail: filipe.vinci@centralesupelec.fr).

II. Modeling of the EGR valve

The EGR valve is an eloquent example of a complex compact actuator. The primary function of this device is to reduce the amount of nitrogen oxide particles at the Internal Combustion Engine (ICE) outlet by substituting exhaust gases for a part of the intake fresh air. An electromechanical device is used to obtain EGR flow air requested by the vehicle computer. This paper uses the optimization of the EGR valve to illustrate a sizing methodology that handles complex multiphysics problems by applying an evolutionary algorithm and parallel computing.

The topology of the EGR valve is illustrated in Fig. 1. The amount of exhaust gases injected is controlled using a flap (the load), driven by a DC motor coupled to a gear. This actuator is driven by a DC-DC converter (an H-bridge), with power supplied by the car battery. A control algorithm, implemented on a microcontroller, modulates the duty cycle of the H-bridge so that the position of the flap is regulated. The pulsed modulation generates conducted electromagnetic interferences on the supply lines that must be suppressed by the addition of an EMC filter.

Automotive components are often exposed to harsh thermal environment [4]. In the case of the EGR valve, the exhaust gases flowing through the device and the proximity of the ICE result in a high ambient temperature. This forces us to consider the thermal behavior of our system in its environment to be of utmost importance. Several physical domains must be considered simultaneously by the optimization process in order to find the best solution. In this paper, the process will aim at the volume minimization of the system. To maximize the embedded power density allows for integration within strictly constrained space conditions in the vehicle, which poses a major challenge in automotive industry.

The system volume is mainly due to the machine and its transmission. Transmission will be considered as a fixed parameter even if its sizing could be treated with the same optimization with an appropriate modeling. However, the machine volume can be reduced, only if its electrical current is increased. This current will not affect significantly the size of the converter itself, but it can impact the size of the filter, as well as the switching frequency. For this reason, the objective will be the reduction of the sum of the filter and the machine volumes.

The number of equations and couplings is too large to allow solving for an optimized set of parameters using a classic approach. Fig. 2 shows the modeled domains and how they are coupled in our system.

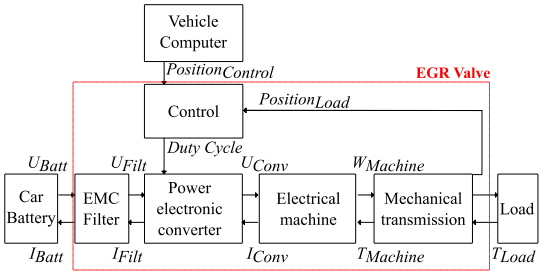

Fig. 1. EGR valve as a compact actuation system.

A Differential Evolution (DE) algorithm [5] is chosen to optimize the system as gradient methods cannot be used on such complex coupled models. Moreover, a non-deterministic approach allows us to reach a global optimal solution rather than a local optimum.

In the next subsections, each model will be detailed.

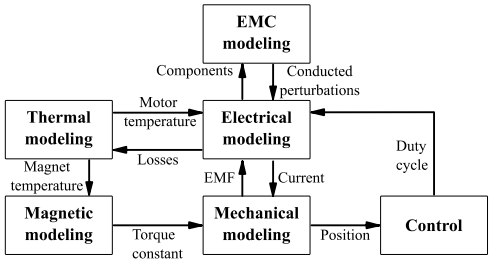

Fig. 2. Interaction between the various models.

A. Electrical model

The electrical model illustrated on Fig. 3 is divided into two parts. The first part concerns the DC machine: an inductor L_{Motor} in series with a resistor R_{Motor} are representative of the low-frequency impedance of the machine. The mechanical reaction introduces the counter electromotive force *EMF*.

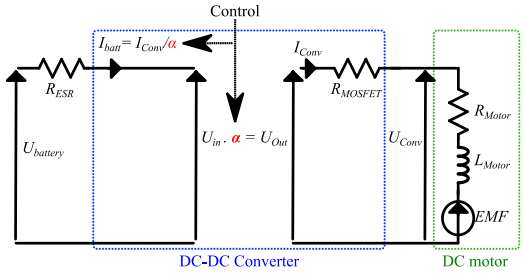

Fig. 3. Electrical linear modeling.

However, the actuator is considered to be in locked-rotor state. This assumption is consistent with the expected functional behavior of the system since it is supposed to maintain a position. The current absorbed by the motor and the value of the equivalent resistor are the basis for the evaluation of the Joule losses due to the DC motor.

The second part of the model represents the power converter. An averaged model is sufficient to provide the electrical outputs and the various losses in the electrical system. The converter voltages and currents are linked by a simple linear relation involving the duty cycle α. The value of this parameter is given by the control model. An equivalent series resistance R_{ESR} is added to take into account the voltage drop between the battery voltage $U_{battery}$ and the input voltage seen by the converter, U_{in}. The DC-DC converter model includes a serial resistance at its output, R_{MOSFET}, to represent the voltage drop due to the MOSFET on-state resistance.

B. Thermal model

Our application utilizes some simplifications and hypothesis in the thermal model. Temperature differences cause air movements, promoting heat transfer. Due to the small size of the system and to the fact that the rotor is in a static locked state, the convection will be neglected. For the same reasons,

radiation will be neglected even if this assumption could be a source of error, as stated in [6]. Hence, heat transfer will be modeled as conduction. Because of the lack of information at the pre-sizing step, contact thermal resistances are not considered.

The H-bridge structure is composed of four power MOSFET switches. Heat flux produced by the switches is evacuated through the PCB and by natural convection. Conduction and switching losses in the MOSFETs are calculated according to classical equations based on the components characteristics and the switching frequency. The study context considers copper losses (Joule heating) in the motor windings, defined by the coil turn number and the winding dimensions, all other kinds of heating sources in the machine are ignored.

The various parts of the DC motor and the H-bridge were modeled using thermal resistances and thermal capacities, assembled in 3D, as shown on Fig. 4. The implementation (using an LTspice IV hierarchical netlist) contains hundreds of nodes.

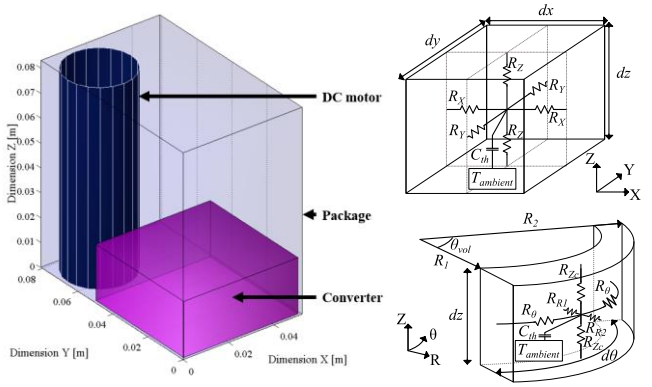

Fig. 4. System topology and elementary thermal volumes.

Both motor and converter models are coupled through a 3D-box, which represents the plastic package of the whole system. The box surfaces, the DC motor and the converter are air-spaced. The outer temperature (ambient temperature) has to be fixed by the designer, and the heat transfer between the box and its environment is modelled by convection. Electrical and thermal data were collected on an industrial prototype to validate the relevance of the electro-thermal model introduced in this subsection and the previous one.

The measurements were performed at a 22°C ambient temperature. The converter and the DC motor were supplied in an open-loop configuration, with a locked-rotor state. The duty cycle was approximately 0.21 under a supply voltage of 12V. The whole system was packaged as shown on the Fig. 5.

The evolution of the motor current and voltage must be compared to a measurement result, since these are the sources of the main losses in the system, and thus the input data for the thermal model: the results are shown in Fig. 6.

The temperatures obtained by simulation and experimental measurement on the motor case and on the MOSFET packages can be compared using Fig. 7. Overall, experimental and simulation results match satisfyingly. However, the evaluation of the MOSFET package temperature is well below the measured value. Our modeling hypotheses introduced above are clearly too coarse w.r.t. local thermal phenomena (convection and radiation) at the MOSFET scale. This is the most likely explanation for this discrepancy.

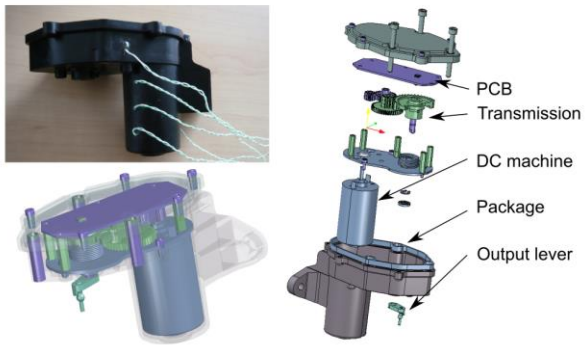

Fig. 5. Top left: actuator with thermocouples inserted through the package. Bottom left: closed 3D drawing. Right: exploded view.

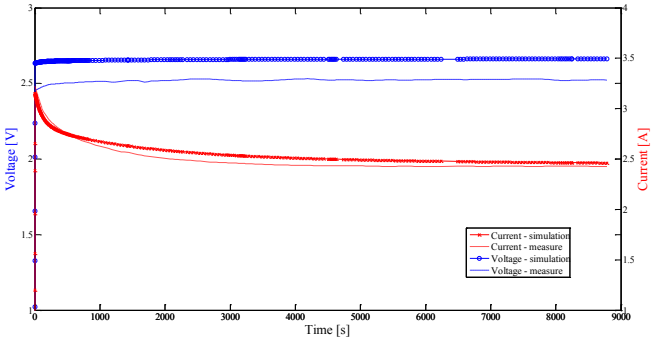

Fig. 6. DC motor current and voltage. Comparison between measurements and simulation results.

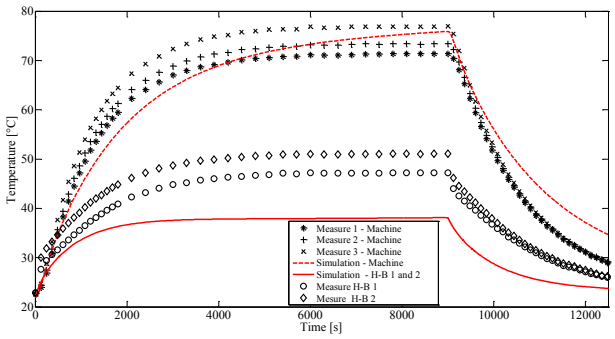

Fig. 7. DC motor case temperature and MOSFET case temperature. Comparison between measurements and simulation results (H-B means H-bridge).

C. Magnetic model

DC motor performances are influenced by its thermal environment, through the behavior of the permanent magnets. A simple linear analytical model, based on [2], is used to take into account the temperature of the magnets extracted from the thermal model to deduce the torque constant available in the motor. Equation (1) takes into account the impact of the temperature on the magnet behavior. The flux density of the magnet *B*r is given in (1) as an affine function of the temperature *Temp*, with an offset B_r^{offset} and a slope B_r^{slope}.

$$B_r = B_r^{offset} + Temp.B_r^{slope} \quad (1)$$

The flux density in the air gap B_e can be deduced from B_r using (2).

$$B_e = \frac{B_r . e_a}{\mu_a . e_{magnet} + k_{ea} . e_a} \quad (2)$$

Where e_a and e_{magnet} are respectively the air gap and the magnet thicknesses. μ_a is the relative permeability of the magnet and k_{ea} is the concentration coefficient of the magnetic flux φ. Then, φ can be deduced using the equation (3).

$$\varphi = B_e . T_a . \pi . r_{er} . l_{rotor} \quad (3)$$

Where the aperture angle of the induction pole intervenes through the coefficient $T_a.\pi$. r_{er} and l_{rotor} are respectively the radius and the length of the rotor. Finally (4) gives the torque constant where n is the number of winding turns in the motor.

$$K_t = \frac{\varphi . n}{2 . \pi} \quad (4)$$

D. Mechanical model

Simple analytical equations allow the connection between the electrical characteristic of the DC motor and its mechanical behavior. The torque T_{motor} can be deduced from the torque constant K_t and the current in the motor I_{motor}, according to (5).

$$T_{motor} = K_t . I_{motor} \quad (5)$$

The motor speed ω_{motor}, the resistive torque T_{res} and the motor torque are linked by (6), where J_{mec} is the mechanical total inertia seen by the motor shaft.

$$\frac{d\omega_{motor}}{dt} = \frac{T_{motor} + T_{res}}{J_{mec}} \quad (6)$$

Then the position of the flap can be deduced easily using (7).

$$\theta_{flap} = \frac{1}{red} . \int \omega_{motor} . dt \quad (7)$$

Where *red* is the reduction ratio of the gear.

E. Control model

Implementing an EGR control loop enables the designer to check key design requirements of the system, such as the response time, static or dynamic position errors. A typical control system has been implemented in our model: a Proportional Integrator (PI) control with a filtered input. In our case, the objective is to monitor the position of the flap. The control parameters are defined using the system parameters. The time constant of the control T_i is deduced from the time constant of the system T_Σ using (8).

$$T_i = 10 . T_\Sigma = 10 . \frac{R_{motor} . J_{mec}}{K_t^2} \quad (8)$$

If the DE algorithm changes the geometry of the machine, the value of J_{mec}, K_t or R_{motor}, then the control parameters are recalculated. The static gain H_0 is given in (9).

$$H_0 = \frac{1}{K_t . red} \quad (9)$$

Finally, the proportional term K_p of the control is calculated thanks to (10), where T_{resp} is the expected response time of the system. The system must meet a mission profile, depicted on Fig. 8.

$$K_p = \frac{10}{T_{resp} . H_0} \quad (10)$$

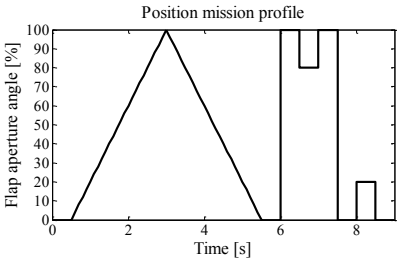

Fig. 8. Position mission profile defined for the EGR valve.

F. EMC model

Automotive systems engineer wish to benefit from an early integration of the EMC constraints in their design process. Nowadays, the control of automotive electromagnetic interference is essential. Conducted interferences have to be maintained within the limits allowed by EMC standards. Our automotive application is subject to the CISPR25 EMC standard [7], which addresses a frequency range from 150kHz to 108MHz.

Filtering is a widely used approach where the potential victim is protected against the interferences thanks to an EMC filter. However the filtering components (inductors and capacitors) can account for a large part of the total volume of the product: the lower the frequency to filter, the larger the component is. Ignoring the EMC constraints during the development process can lead to a functional product, but which does not meet the normative requirements. Therefore the whole sizing has to be reconsidered or a bulky filter has to be inserted, posing the risk of sacrificing the compactness of the system.

For this reason, our study aims at limiting the interference emitted within a frequency range from150kHz to 10MHz, in order to avoid this EMC compliance risk. Beyond this limit of 10MHz, the EMC filter can be unobtrusively sized without particular precautionary measure concerning the volume of the components. Passive components are characterized using a Vector Network Analyzer (VNA) [8], and their impedances, deduced from these measurements, are matched to equivalent models, as illustrated in Fig. 9. PCB and wiring parasitic impedances are not considered, given the frequency domain addressed in this study.

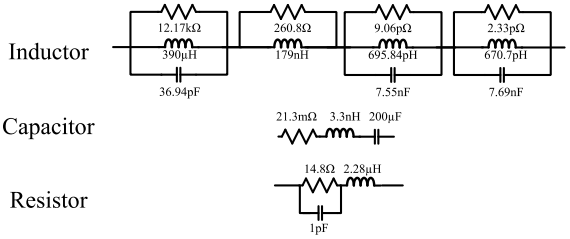

Fig. 9. Equivalent models of passive components for high frequency simulation.

Our approach uses a direct simulation in the frequency domain, implemented in the LTspice IV simulator. The interference sources are modeled by equivalent current and voltage sources.

The brushed DC motor and the MOSFET components are the main interference sources because of their switching behaviors. However, the DC motor is considered to be in locked-rotor state. Consequently, it is modeled as a passive impedance (measured with a VNA) and matched to the equivalent model given in Fig. 9 [9].

MOSFET are assimilated to a variable resistance (R_{DSon}/ R_{DSoff} in on/off-states), associated with a parasitic serial inductor and a parasitic parallel capacitor. This complexity level is sufficient to deal with our restricted frequency range. In the frequency domain, this amounts to injecting a trapezoidal waveforms as interference sources. The corresponding Laplace transform is given in (11).

$$V(f) = \frac{A.2\pi}{T}.\left(\frac{1-e^{-t_{rise}.p}}{t_{rise}.p^2} - \frac{1-e^{-t_{fall}.p}}{t_{fall}.p^2}.e^{\left(-\tau-\frac{t_{rise}-t_{fall}}{2}\right).p}\right) \quad (11)$$

Where A is the magnitude of the signal, t_{rise} and t_{fall} are respectively the rise time and the fall time of the interference waveform. T is the switching period and τ is the time during which the signal is greater than $A/2$. To model the electrical power supply system of the vehicle, a Line Impedance Stabilization Network (LISN) is necessary. The LISN filter is implemented in our model using the device datasheet model as shown in the schematic of Fig. 12. To limit the conducted interference emitted by the system, a Gamma EMC filter is placed at the input of the H-bridge, also illustrated in Fig. 12.

The interference level obtained by the simulation of the model introduced in Fig. 12 is compared to the interference measured on an experimental prototype. The result is given in Fig. 10, which depicts the interference as signal V_{p+}. In this comparison, the Gamma filter is removed in both experimental and simulation systems. The results match up to 1MHz, and the simulation is representative of the experimental results up to 3MHz. To obtain good agreement beyond this frequency, the model would need further refinement.

G. Simulation

The models introduced in this section were coupled together. Some key variables are exchanged, as depicted in Fig. 2. The widely spread time constants in the system would increase prohibitively the computing time of a simulation run. For this reason, a relaxation method is used to simulate the thermal behavior separately from the evaluation of the other domains. The relaxation, illustrated in Fig. 11, allows one to run a simulation of the thermal model apart from the other models, and it provides the electrical model with updated temperatures. Then, corresponding losses are deduced and the thermal model is computed again. This loop tends to converge, and the losses and the temperatures are considered to be solved when their values do not vary anymore in a given tolerance range.

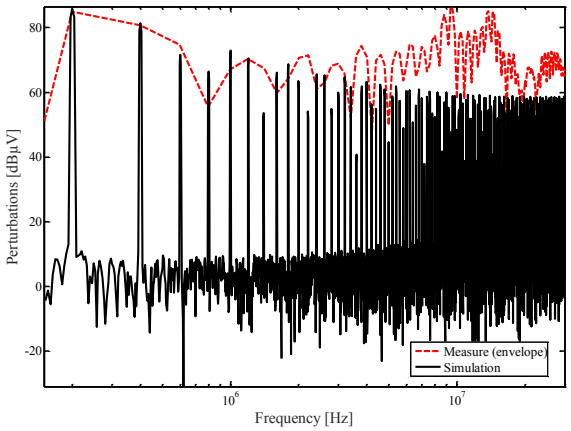

Fig. 10. Measured and simulated interference spectra.

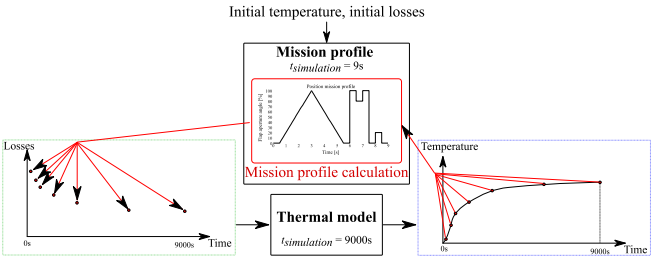

Fig. 11. Electrothermal simulation using a relaxation approach.

III. Optimization

A. Optimization cost, constraints and parameters

The objective of our optimization is to minimize the geometrical size of the system. Three components are taken into account to calculate the global volume of the system: the DC motor, the power electronics converter and the EMC filter. Both DC motor and power converter are considered into the same box: the package. The remaining space in the box would be used to integrate the mechanical gear and the various mechanical elements that are not represented in our model. The volume of the filter is added to the volume of the box and the sum of these components is the objective function to be minimized in our optimization, as detailed in (12).

$$Volume = L_{box}.h_{boc}.e_{bax} + V_L + V_C \quad (12)$$

Where L_{box}, h_{box}, and e_{box} are respectively the length, the height and the depth of the package which contains the DC motor and the power converter. V_L and V_C are the volumes of, respectively, the inductor and the capacitor of the EMC filter.

Several constraints are considered. First, the capability of the system to meet the functional requirements must be ensured. The system is expected to respect the mission profile defined on Fig. 8. The response time at 90% of the final value must be less than 150ms. This criterion is evaluated during the step input at *time*=6s. Moreover, the dynamic error of the flap position during the ramp phases (between *time*=0.5s and *time*=5.5s) must be less than 3%. In order to limit the mechanical torque ripple, the current ripple in the DC machine must be less than 10% of the current mean value.

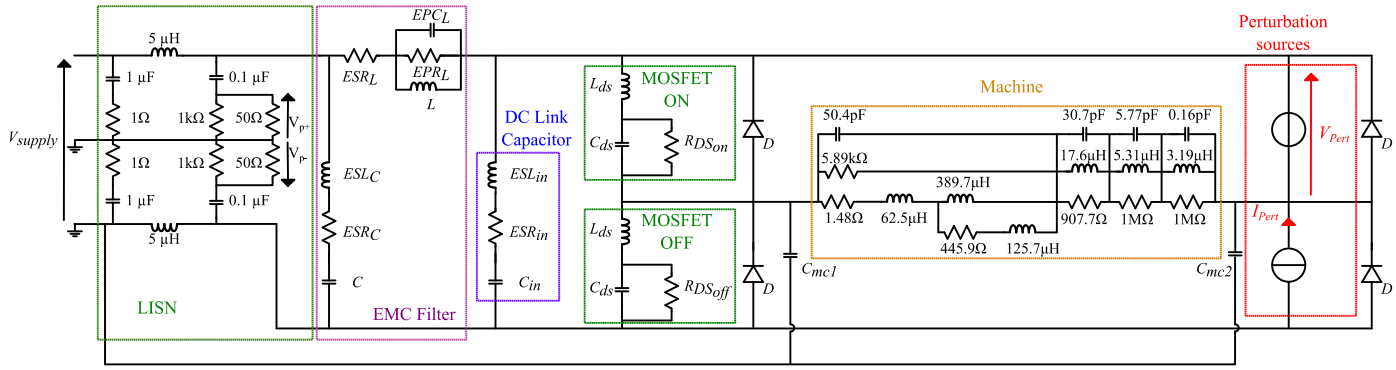

Fig. 12. EMC model of the H-bridge converter associated with the DC motor, the Gamma filter and the LISN.

Thermal constraints must be considered too. The first one concerns the magnet temperature in the machine. To limit the loss of performances due to their increasing temperature, a maximal magnet temperature of 140°C is imposed. To avoid the risk of damage in the power converter, the MOSFET case temperature should not exceed 80°C. Although this constraint may seem severe, it allows to anticipate the situation where the MOSFET selected later frequently presents poor performances (high on-state resistance, high junction-to-case thermal resistance), because of availability or lower cost.

The last constraint concerns the compliance with the EMC standard (CISPR25). The conducted interference must stay below the maximal value allowed by the standard.

To meet these multiphysics constraints, the DE algorithm can change several parameters. Two of them are geometrical distances: the distance L between the converter and the DC machine, and the thickness of the magnet, e_{magnet}. The increase of L can limit the heating of the MOSFET due to the losses in the machine. The increase of e_{magnet} would allow to reduce the current needed by the machine to respect the mission profile, and so the heating in the converter. In both cases, these benefits are counter-balanced by an increase of the global volume. Other geometrical spaces were also considered, but a previous study [10] showed that all the distances between the converter and the package on one hand, and the machine and the package on the other hand, would be reduced to their minimal value by the optimization. To limit the number of parameters, they are all set to 1mm.

A third sizing parameter is considered: the switching frequency of the converter f_{switch}. The switching losses increase with the frequency but the current ripple and the EMC filter size decrease. The optimization of this parameter should allow the tool to reach an interesting trade-off.

Finally, two other parameters are considered in this optimization: the inductor and the capacitor used in the EMC filter. These components are selected among components referenced in the circuit parts databases, created from experimental characterization. For the purposes of this study, 41 capacitors and 18 inductors were stored, all compliant with automotive specifications (temperature range).

The minimum, maximum and initial values of the parameters are given in the Table I. The maximum and minimum values are set according to the technical feasibility, the mechanical tolerances and the maximum values available in the database. The initial parameter setting must respect the constraints. A large value for L tends to decrease the MOSFET heating, and a maximal e_{magnet} tends to decrease the current, and so the MOSFET heating. A maximal switching frequency will limit the current ripple, but stronger filtering is necessary to limit the EMC interferences. Given the initial settings respecting the constraints, then the volume must be reduced.

TABLE I
OPTIMAL PARAMETERS

Parameter	Unit	Min.	Max.	Init.	Opt
L	mm	1	100	60	4.4
e_{magnet}	mm	1	40	20	1.7
L_{filtre}	H	$2.2e^{-6}$	$4.7e^{-6}$	$4.7e^{-6}$	$4.31e^{-6}$
C_{filtre}	F	$220e^{-12}$	$1e^{-5}$	$1e^{-5}$	$5.6e^{-6}$
f_{switch}	Hz	$2e^{3}$	$2e^{5}$	$2e^{5}$	$28.22e^{3}$
Volume	cm^3	350.82	23000	73710	371.47

An evolutionary algorithm based on DE is used to search for the system's optimum value. The settings of the optimization are as follows: the population includes 50 individuals, the cross factor is 0.9, the mutation coefficient is 0.6 and a maximum number of iteration is 1500 (shutoff parameter in case of non-convergence or slow convergence).

B. Multiphysics optimization of the system

The computing time of the whole optimization is two days. However, mean simulation time is not significant, since the electro-thermal relaxation loop can lead to several simulations for a given set of parameters. Moreover, the constraints with the lower computation cost are checked first to prevent the algorithm from running the heavier simulations with unacceptable solutions. This strategy tends to increase the computing time of a generation as the optimization converges towards the optimal solution. In any case, two days represents a significant improvement compared to the effort that would be needed for pre-sizing an EGR without optimization process, with a comparably degree of accuracy. Nevertheless, this computing time could be easily reduced using parallelization, since the main simulation software is LTspice IV, which can profit cheaply from virtualization of computing nodes, in the cloud.

The Table I gives the optimal parameters found and the optimal volume of the system. The optimal solution shows reduced distances L and e_{magnet} in comparison with the initial values. Concerning the choice of the filter components, the database contains commercially available values: our algorithm uses continuous values and the components with the nearest

value in the database are chosen and, then, used in the simulation. Thus the optimal values for the capacitor and the inductor (respectively 5.6µF and 4.31µH) lead to the closest components in the database, whose values are respectively 4.7µF and 4.7µH . The switching frequency is reduced from 200kHz to 30kHz.

This optimal solution meets the various constraints in the system. To determine the influence of the temperature on these constraints; five evaluations of the performances are done at five different instants during the thermal simulation. Fig. 13 shows the copper temperature in the DC motor and the five points in time selected. The complete thermal simulation time is 4000s, which corresponds to the time needed to reach the thermal steady state in the case where the geometrical parameters tend to maximize the volume.

The optimal system complies with the thermal constraints. Fig. 13 shows that the magnet temperature is always less than 140°C, and the MOSFET case temperatures do not exceed 80°C. The limiting constraint is the MOSFET temperature, whereas the weakness of the thermal model on this very point has been highlighted. For this reason, it is deemed necessary to keep a significant safety margin concerning the value of the constraint. Given the losses level in the component, we know the component can tolerate a case temperature of up to 110°C, but the inaccuracies in our thermal modeling prompts us to limit this temperature to 80°C. An improved thermal model would possibly make the optimal selection of the MOSFET part more realistic.

Whatever the thermal conditions during the profile, the response time is 115ms, and thus less than 150ms. Dynamic error is less than 2.4%, and thus less than the 3% maximum error. The values reached by the parameter L during the optimization explains why the MOSFET temperature are exactly at the limit given by the constraint. Fig. 14 shows the current in the DC motor. The ripple is 143mA, and the mean value is 1.427A. The relative current ripple is then 10%, so it matches with the limit given by the constraint. As far as possible, the optimization leads to the reduction of the switching frequency, helping the EMC interference reductions.

Indeed, Fig. 15 shows that the interference obtained is below the limits required by the standards. To obtain this interference spectrum, the choice of the filter components is essential. One can observe in Fig. 15 that without the optimal filter, the interference would exceed the CISPR25 (class 5) standard limit, at 150kHz. Each time correspond to an increase of the magnet temperature of a fifth of the global magnet heating. The response time is still 115ms at any moment and does not depend on the temperature.

As expected, the filter given by the optimization algorithm is one of the most compact filters possible with the available components. It is composed of a capacitor of 4.7µF in a Surface Mounted Device package, and an inductor of 4.7µH. The global volume of the filter is mainly due to the inductor. The filter volume is 1.22cm^3, whereas the global volume of the system is 371.46cm^3. Thus the filter represents only 0.33% of the system volume.

This observation leads one to realize that the parameters e_{magnet} and L are of utmost importance for the definition of the global volume. The tool had no prior information of this. Nevertheless, our approach assures the designer that the filter obtained is one of the smallest possible, given the parts database considered. Indeed, the 738 possible filters have been simulated and their volume is represented on Fig. 16, as a function of the margin available with respect to the standard limit. The optimization algorithm found a filter of minimal volume without consideration for the margin maximization. A bi-objective optimization could be an interesting improvement to the method.

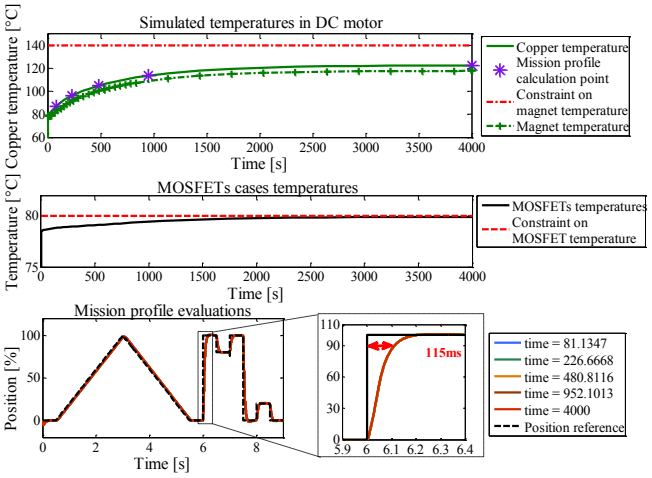

Fig. 13. Mission profile matching with simulation results at five different times.

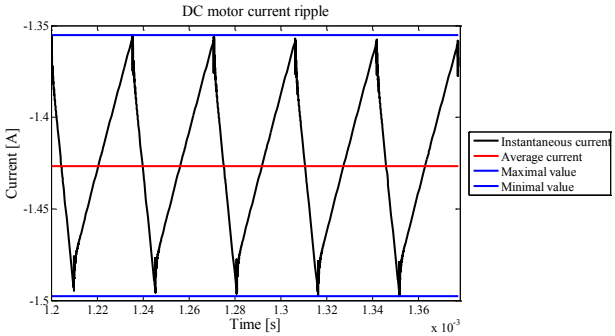

Fig. 14. Current waveform in the DC motor. Current ripple is exactly at 10% of the current mean value.

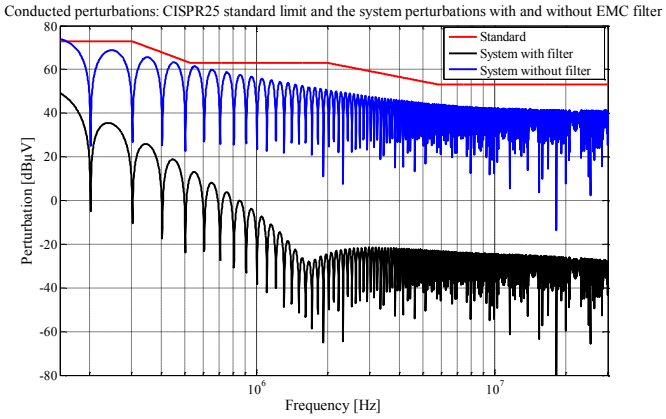

Fig. 15. EMC conducted interferences with and without EMC filter compared with the standard limits. The filter is necessary.

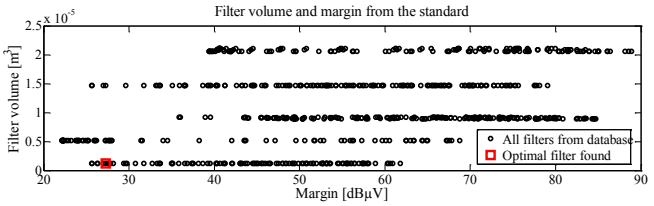

Fig. 16. Volume of the 738 filters as a function of the deviation from the standard. The volume discretization is due to the preponderance of the inductor volume.

IV. Conclusions

We can conclude that the optimization algorithm solved the trade-off to size the system. The feasibility of applying an evolutionary algorithm to pre-size a multiphysics system typical of automotive applications has been demonstrated. It is important to note that the effectiveness of the approach is linked to the quality of the various models, and the strategy employed to couple them into a global simulation. More accurate modeling can lead to a fine-tuning optimization run for parameter determination.

But inherent precision is not sufficient: the multiphysics approach requires a consistent precision level among the modeled domains. Indeed, accuracy leads to increased computing times, but accurate inputs from one domain for less accurate models in another can be considered as a waste of time.

For this reason, an improvement in this optimization approach could be to raise the global precision of the various models. Because of the computing time resulting from this, an adaptive parallelization of the simulation run should be considered. Gradual accuracy optimizations could be used to reduce progressively the search space, using models with varying degrees of complexity.

Lastly, the impact of the optimization in a pre-sizing step on the industrial final product remains an open question. Indeed, several constraints such as costs, availability, obsolescence, or reliability can affect the ultimate design. From an industrial point of view, the integration of these constraints into the same global approach would constitute the ultimate goal to achieve.

References

[1] "European union official journal from European parliament and council of 20th june 2007: law (ce) n715/2007."

[2] C. Gutfrind, P. Dessante, P. Vidal, J-C. Vannier, "Analytical study of an optimized limited motion actuator for automotive application used in engine combustive flow regulation" in *Electrical Review journal*, issue 7b-2012 ISSN0033-2097

[3] M. Bendali, C. Larouci, T. Azib, C. Marchand, and G. Coquery, "Design with optimization of an interleaved buck converter for automotive application; effect of the EMC constraint," in *7th IET International Conference on Power Electronics, Machines and Drives (PEMD 2014)*, DOI 10.1049/cp.2014.0260, pp. 1–6, Apr. 2014.

[4] M. Ohadi and J. Qi, "Thermal management of harsh environment electronics," in *Twentieth Annual IEEE Semiconductor Thermal Measurement and Management Symposium, 2004*, DOI 10.1109/STHERM.2004.1291329, pp. 231–240, Mar. 2004.

[5] K. Price, R. M. Storn, and J. A. Lampinen, *Differential Evolution: A Practical Approach to Global Optimization (Natural Computing Series)*. Secaucus, NJ, USA: Springer-Verlag New York, Inc., 2005.

[6] F. F. Wang, "Electronics packaging simplified radiation heat transfer analysis method," in *The Ninth Intersociety Conference on Thermal and Thermomechanical Phenomena in Electronic Systems, 2004. ITHERM '04*, DOI 10.1109/ITHERM.2004.1319232, pp. 613–617 Vol.1, Jun.2004.

[7] *International Electrotechnical Commission, CISPR25: Radio Disturbance Characteristics for the Protection of Receivers Used on Board Vehicles. Boats and on Devices-Limits and Methods of Measurement*. IEC, 2008.

[8] M. Bensetti, F. Duval, and B. Ravelo, "Thermal effect modeling on passive circuits with MLP neural network for EMC application," *Progress In Electromagnetics Research M*, vol. 19, DOI 10.2528/PIERM11042602, pp. 39–52, 2011.

[9] F. Diouf, F. Leferink, F. Duval, and M. Bensetti, "Wideband Impedance Measurements and Modeling of DC Motors for EMI Predictions," *IEEE Transactions on Electromagnetic Compatibility*, vol. 57, DOI 10.1109/TEMC.2014.2370454, no. 2, pp. 180–187, Apr. 2015.

[10] F. Robert, F. V. D. Santos, C. Gutfrind, L. Dufour and Ph. Dessante, "Multi-physics optimization of a smart actuator for an automotive application", in *17th European Conference on Power Electronics and Applications (EPE'15 ECCE-Europe)*, DOI 10.1109/EPE.2015.7309129, pp. 1–10, Sep. 2015.

Florent Robert received the Ph.D. degree in electrical engineering from the Université Paris-Saclay, France, in 2015. He is currently a research engineer in system optimization for the Advanced Research Department of the French car manufacturer supplier EFi Automotive. His research interests include multiphysic modeling, validation and optimization of actuation systems.

Mohamed Bensetti was born in Algeria, in 1973. He received his Master Research degree in 2001 and his Ph.D. in electrical engineering in 2004 from the University of Paris-Sud, France. He received the accreditation to supervise research from the University of Paris-Sud in 2014. In 2007, he joined the ESIGELEC and the IRSEEM laboratory. Since 2013, he is with CentraleSupélec and the GeePS laboratory. His domains of research are modeling, simulation and instrumentation in electromagnetic compatibility and power electronics.

Filipe Vinci dos Santos earned his B.Sc. (electronics engineering) and M.Sc. (microelectronics) from the Federal University of Rio de Janeiro in 1989 and 1992, respectively, and his Ph.D. degree (physics-microelectronics) from the University of Grenoble I, France in 1998. Since 2010 he holds the Chair on Advanced Analog Systems at CentraleSupélec. His research interests are aerospace, automotive and biomedical systems where the interaction between electronics and the surrounding environment is a fundamental design concern.

Laurent Dufour received a Technology University degree in Physical Measurements and joined the company Electricfil Automotive in 1984. Through numerous R&D projects, he studied many sensor and actuator technologies, for their integration into industrial automotive field applications. He is currently responsible for the electromechanical conversion system design team of the Advanced Research department, EFi Automotive. His work focuses on the development of design and optimization methods for the sizing of actuation systems.

Philippe Dessante was born in 1971. He studied applied mathematics and physics at Montpellier and Versailles universities. He received his PhD in 2000 for his work on streamer type electric discharge modeling from the Versailles University. He got is accreditation to supervise research in 2012 on electrical systems design and modeling. He is currently Professor at CentraleSupélec. His main research topics are simulation and optimization of electrical systems.